

High photon flux Kα Mo x-ray source driven by a multi-terawatt femtosecond laser at 100 Hz

Y. Azamoum, R. Clady, A. Ferré, M. Gambari, O. Uteza, M. Sentis

▶ **To cite this version:**

Y. Azamoum, R. Clady, A. Ferré, M. Gambari, O. Uteza, et al.. High photon flux Kα Mo x-ray source driven by a multi-terawatt femtosecond laser at 100 Hz. Optics Letters, 2018, 43 (15), pp.3574. 10.1364/OL.43.003574 . hal-02137923

HAL Id: hal-02137923

https://amu.hal.science/hal-02137923

Submitted on 23 May 2019

HAL is a multi-disciplinary open access archive for the deposit and dissemination of scientific research documents, whether they are published or not. The documents may come from teaching and research institutions in France or abroad, or from public or private research centers.

L'archive ouverte pluridisciplinaire **HAL**, est destinée au dépôt et à la diffusion de documents scientifiques de niveau recherche, publiés ou non, émanant des établissements d'enseignement et de recherche français ou étrangers, des laboratoires publics ou privés.



Distributed under a Creative Commons Attribution 4.0 International License

Optics Letters

High photon flux K_α Mo x-ray source driven by a multi-terawatt femtosecond laser at 100 Hz

Y. Azamoum,* R. Clady, A. Ferré, M. Gambari, O. Utéza, and M. Sentis

Aix Marseille Univ., CNRS, LP3, Marseille, France
**Corresponding author: azamoum@lp3.univ-mrs.fr*

Received 24 May 2018; accepted 15 June 2018; posted 26 June 2018 (Doc. ID 332500); published 19 July 2018

We develop a pulsed hard x-ray K_α source at 17.4 keV produced by the interaction of a multi-terawatt peak power infrared femtosecond laser pulse with a thick molybdenum (Mo) target at a 100 Hz repetition rate. We measure the highest Mo K_α photon production reported to date corresponding to a K_α photon flux of 1×10^{11} ph/(sr·s) and an estimated peak brightness of $\sim2.5\times10^{17}$ ph/(s·mm^2·mrad^2 (0.1%bandwidth)) at $\sim5\times10^{18}$ W/cm^2 driving laser intensity. © 2018 Optical Society of America

OCIS codes: (340.7480) X-rays, soft x-rays, extreme ultraviolet (EUV); (140.7090) Ultrafast lasers; (350.5400) Plasmas.

https://doi.org/10.1364/OL.43.003574

The interest in developing brilliant, ultrashort, compact, and reliable hard x-ray sources at a reduced cost and laboratory size is motivated by a growing number of societal and scientific applications such as non-destructive testing in industry, biomedical imaging, or probing ultrafast lattice dynamics and phase transitions in material science [1,2]. In addition to conventional accelerator-based x-ray sources of high brightness and femtosecond time resolution, laser-driven plasma x-ray sources are a practical alternative with a relative low cost, a reduced footprint, and an intrinsic synchronization for pump and probe experiments. Among different laser plasma x-ray sources, K_α sources have been developed for decades for applications such as x-ray absorption spectroscopy [3], and x-ray diffraction [4], or phase contrast imaging [1]. Indeed, the main benefits are their simplicity and reliability. Moreover, they are complementary to the emerging high brightness x-ray sources produced from laser gas jet interaction like betatron radiation [5] and Compton backscattering x-ray source [6], which require intense and energetic laser sources (> several tens of terawatts). Unfortunately, today they are limited in terms of repetition rate to a maximum of ~10 Hz.

The K_α hard x-ray source is produced by the interaction of a relatively intense laser beam ($I > 10^{16}$ W/cm^2) with a high atomic number Z solid target. The generation of the K_α lines involves a number of physical processes such as ionization, plasma expansion, several collisionless absorption mechanisms generating hot electrons, the scattering of these electrons in the solid and K-shell ionization. For optimal use of K_α sources for applications, the key parameters are a high photon flux, a point-like x-ray source, and an ultrashort x-ray pulse duration. To get access to these characteristics and, especially, to reach a high photon flux per shot, operation of the driving laser at high intensity is needed [7], requiring the use of multi-terawatt femtosecond laser sources. The efficient generation of K_α hard x-ray photons (>10 keV) necessitates even higher intensity when the atomic number Z of the target increases, as empirically scaled [8]. A high repetition rate of the driving laser pulse is also an important parameter to reduce the time exposure or the dose delivered while accessing to suitable (high) and flexible signal-to-noise and contrast-to-noise ratios for applications in the context of medical imaging [9] or material science [10]. Many research groups developed K_α sources at a high repetition rate reaching 1 kHz [3,11]. However, these systems are limited in laser energy per pulse which precludes the delivery of high intensity on target and, thus, reduces the conversion efficiency and the total hard x-ray flux [7,12]. At the opposite, high-energy ultrashort laser sources are limited to a low repetition rate [12,13] which is an obstacle when time exposure or sensitivity to x-ray peak dose is a concern. In this Letter, we propose to pave an intermediate way combining a mid-x-ray dose per pulse, requiring multi-terawatt driving laser system, and a relatively high repetition rate (>10 Hz) for delivering high average power and high brightness x-ray sources which are suitable for many applications. Thereby, we demonstrate an unrivalled performance in terms of the average photon flux of an intense K_α hard x-ray (17.4 keV) source generated with a unique laser system delivering intermediate energy per pulse (~ up to 122 mJ on target) and an ultrashort pulse duration (~25 fs) at the relatively high repetition rate of 100 Hz. Finally, the characteristics of the present Mo K_α x-ray laser plasma source are compared with those published to date.

The K_α x-ray source is generated using a p-polarized beamline (nominal performances: 800 nm, 220 mJ, 25 fs, 100 Hz, ns temporal contrast ratio (CR) $I_{\text{peak,fs}}/I_{\text{background,ns}} = 10^{10}$) of LP3-ASUR facility [14]. Experimental details of the driving laser source, beam transport to the Mo target, and x-ray source diagnostics can be found in Refs. [7,14]. We recall hereafter only specific points related to running such experiments at 100 Hz. We first measured a pulse-to-pulse energy stability of 2% rms at 100 Hz. We also evaluated the importance of wavefront aberrations induced by the laser average power

developing in the compressor and in beam transport optics related to the operation of the 100 Hz–multi-terawatt laser driving source. We observe that, even at high average power (>10 W), the thermally induced wavefront aberrations have no time to develop for a reduced number of shots (typically ~1000 shots – 10 s) [14]. In this Letter, in order to evaluate the performance of our x-ray source as a function of the driving intensity, we thus limit the number of shots to 1000 when the average power exceeds 10 W. To generate the x-ray source, the laser beam is focused at an angle of incidence of 45° by an off-axis parabolic (OAP) mirror (effective focal length = 150 mm) on a rotating thick molybdenum (Mo) disk (6 mm thickness and 100 mm in diameter) with a polished surface (roughness < 1 μm). The focused spot size is 4.8 μm × 7.7 μm full width at half-maximum (FWHM) with more than 64% of laser pulse energy being within $1/e^2$ of peak intensity level. The laser intensity is adjusted by varying the pulse energy using a half-wave plate and a polarizer located in the final power amplifier of the laser chain. To optimize the service of the target, a spiral displacement is provided using motorized rotating and vertical translation stages synchronized with the laser source. To ensure a fresh target surface for each laser pulse at 100 Hz, we adjust the velocity of the motorized stages to get a distance of typically 100 μm between two consecutive laser shots. Under these conditions, the target lifetime corresponds to ~10^6 laser shots.

The targetry system is managed to ensure an optimized shot-to-shot repeatability at 100 Hz. The deviation to perfect flatness of the polished Mo disk is measured to be <15 μm with a confocal microscope considering the whole surface. The perpendicularity of the target to the optical laser beam axis can be rectified for any position of the target along the optical axis with the help of a micro-actuator. Then the verticality of the target surface during the disk rotation and vertical displacement is adjusted *in-situ* with a mechanical-contact position detector and controlled during the experiments with a low depth-of-field (numerical aperture [NA] = 0.4) imaging system. In this way, the position of the target surface is adjusted with the precision of ±15 μm which is much lower than the confocal parameter of the laser (~210 μm). A 100 μm thick and 50 mm diameter glass wafer is positioned perpendicular to the laser beam, at a distance of 3 cm of the OAP to protect it from the debris produced during laser-target interaction. A calibrated photodiode located after the target allows us to monitor the transmission of the wafer, which can be degraded due to the accumulation of debris. When the attenuation is measured higher than 10%, the wafer is replaced. Its lifetime is ~10^4 to 10^6 laser shots, depending on the laser intensity. All these available adjustments promote stable target and laser intensity conditions, which are important in view of operating the K_α x-ray source at a high repetition rate [15].

In Fig. 1, we measure the number of K_α photons N_{K_α} emitted per unit of solid angle (sr) per laser shot for two decades of laser intensity, ranging from ~3×10^{16} to 6.2×10^{18} W/cm^2.

Using an x-ray CCD camera (*PIXIS-XB, Princeton Instruments* –1024 × 1024 pixels of 13 μm × 13 μm pixel size) in the single-photon counting mode and a calibrated procedure [7], the K_α photon number per shot is deduced from the reconstructed x-ray spectrum. The camera is located at 90 cm from the target at an angle of 45° with respect to the normal of the target front side and perpendicular to the laser beam. To reconstruct the K_α Mo spectrum, one shot is needed at high

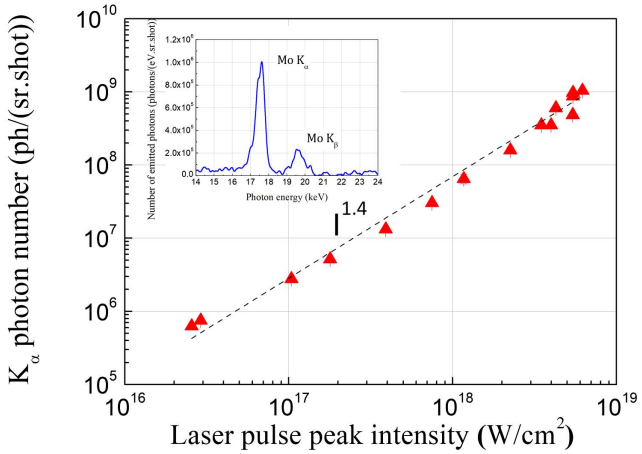


Fig. 1. K_α production as a function of the laser peak intensity. The error bar associated with each value is given by the standard deviation calculated from three independent measurements of the K_α photon production. The inset shows an absolute energy spectrum of the Mo x-ray emission obtained with the x-ray CCD camera for the laser intensity of $I = 3 \times 10^{17}$ W/cm^2.

intensity. Few laser shots are required at low intensity to enhance accuracy, yielding an averaged spectrum. In Fig. 1, we observe a continuous increase of the K_α production (N_{K_α}) reaching 1×10^9 ph/(sr · shot) at the highest laser intensity. It corresponds to a conversion efficiency from laser energy into K_α photons of 1.3×10^{-4} in 2π sr. Considering repeated operation of the x-ray source experiment at 100 Hz and a stable x-ray emission, it corresponds to a photon flux of 1×10^{11} ph/(sr · s) and an average power of the source of 1.8 mW (in 2π sr).

In Fig. 1, we also display a fit to the experimental data curve showing an x-ray production scaling as a function of laser intensity I with a power law $N_{K_\alpha} \propto I^\beta$ with $\beta = 1.4$. This scaling law with $\beta > 1$ has also been reported for target materials of lower Z by Arora *et al.* [16] in the intensity range of 3×10^{16}–8×10^{17} W/cm^2 and for a laser pulse duration of 45 fs. Both results differ from those published in Ref. [8]. In the latter, it was shown an optimum laser intensity of $I_{\text{opt}} = 7 \times 10^9 \, Z^{4.4}$ W/cm^2 for maximum K_α yield, and saturation for intensities higher than I_{opt}. For Mo $Z = 42$, I_{opt} corresponds to the laser intensity of 10^{17} W/cm^2. In the present studied range of intensity, we do not observe such a saturation of the K_α production, even at intensity approaching 10^{19} W/cm^2.

Hereafter, we discuss the scaling $N_{K_\alpha} \propto I^{1.4}$. K_α lines are induced by the hot electron population so that the number of K_α photons N_{K_α} is related to the number of hot electrons N_h by $N_{K_\alpha} = N_{K_\alpha/e^-} \times N_h$ with N_{K_α/e^-}, the number of K_α photons produced by one hot electron. N_h can be expressed as a function of the fraction of laser energy absorbed by hot electrons η_h, the hot electron temperature T_h, and the laser energy E_L from the relation [17] $\eta_h \times E_L = N_h \times T_h$. Thus, N_{K_α} can be written as $N_{K_\alpha} = N_{K_\alpha/e^-} \times \frac{\eta_h E_L}{T_h}$. N_{K_α/e^-} has been experimentally determined as a function of the electron energy E [18] using a monoenergetic electron beam up to 40 keV and for a Z material target between 14 and 47. The authors found a scaling of N_{K_α/e^-} as a function of electron energy E and the K-shell ionization energy E_K expressed as $N_{K_\alpha/e^-} \propto (E - E_K)^{1.63}$.

From a Monte-Carlo simulation [8], it was found that this formula fits well with the calculations in the electron energy range 25 keV–1 MeV and for a high Z element such as silver Ag, $Z = 47$. For Mo element ($Z = 42$ and $E_K = 20$ keV) and in the electron energy range (up to several 100 keV) corresponding to the explored intensity range in our experiment, the formula becomes $N_{K_\alpha/e^-} \propto E^{1.72}$. To derive the number of K_α photons emitted per hot electron N_{K_α/e^-}, we consider that the electron energy distribution can be represented by a monoenergetic electron distribution with energy that corresponds to the most probable energy in the Maxwell distribution describing the hot electron population. With the present approximation, we can replace E in the formula with the hot electron temperature T_h for which convenient scaling can be derived. Thus, N_{K_α} can be written as $N_{K_\alpha} \propto \eta_h E_L T_h^{0.72}$. T_h may be further related to the laser irradiance $I \times \lambda^2$ if the absorption mechanism is known. In a previous work, [7] we demonstrated experimentally that for a high CR (CR > 10^9) in the non-relativistic intensity regime ($I < 2 \times 10^{18}$ W/cm^2) the dominant absorption mechanism is vacuum heating [19] while, in the relativistic regime ($I > 2 \times 10^{18}$ W/cm^2), the dominant absorption mechanism is $J \times B$ heating [20]. As found in literature, T_h scales with $(I \times \lambda^2)^\alpha$ where $\alpha = 1/3 - 1/2$, depending on the intensity regime. In the non-relativistic intensity regime and for femtosecond pulse duration [21], the temperature T_h follows the scaling for vacuum heating absorption mechanism with $\alpha = 1/3$ while in the relativistic regime $\alpha = 1/2$ as theoretically predicted [20]. Therefore, N_{K_α} can be written as $N_{K_\alpha} \propto \eta_h I^{1+\alpha 0.72}$. For the parameter η_h, to the best of our knowledge, no scaling was derived in an extended intensity regime as in this Letter. Nonetheless, in particle In cell (PIC) simulations [22] and for similar interaction conditions, it was found that η_h is more or less independent of the laser intensity. Thus, using such approximation we get $N_{K_\alpha} \propto I^{1+\alpha 0.72}$. As a consequence, in the non-relativistic regime, the scaling equation becomes $N_{K_\alpha} \propto I^{1.24}$ while, in the relativistic intensity regime, $N_{K_\alpha} \propto I^{1.36}$. Even though the obtained scalings are derived using approximations, the values of 1.24 and 1.36 are in good accordance with the value of 1.4 obtained from the experimental data in Fig. 1.

In order to progress in the characterization of our x-ray source, we measure its vertical and horizontal size (Fig. 2) as a function of laser intensity using the knife edge method [23]. A sharp Tungsten edge (<0.2 μm roughness) is positioned at 6 cm from the target resulting in an image magnification factor of ∼15 with a spatial resolution of ∼3 μm to extract the x-ray source size. The knife edge image is obtained after accumulation of thousands of laser pulses on the target at low intensity, but with a reduced number of pulses (<1000) when the intensity is sufficiently high ($\geq 2 \times 10^{17}$ W/cm^2). The edge spread function obtained with this shadowgraphy technique is fitted with a Fermi function. The derivative of the Fermi function gives the line spread function, which is fitted by a Gaussian distribution function with an FWHM that corresponds to an effective x-ray source size. Indeed, the real size of the x-ray source is expected to be smaller than the latter because of the need to accumulate over a large number of shots to define a workable image by this technique.

In Fig. 2, for the lower laser intensity ($I \sim 10^{17}$ W/cm^2), the x-ray source size is small (13 μm × 12 μm) with only enlargement factors of ∼2.7 × 1.5 compared to the laser focal spot size. Then the x-ray source size increases almost linearly as a function of the laser intensity and reaches 73 μm × 85 μm at the highest intensity.

The x-ray source size being larger than the laser focus size has been already reported by many authors [12,24]. The broadening of the x-ray emission area may be explained by various physical phenomena such as electron scattering in the solid, the divergence of the accelerated electron beam or the so-called fountain effect [25,26]. It is worth noting that detailed understanding of this result would require complex simulations, which are beyond the scope of this Letter.

The brightness of an x-ray source is an important parameter for applications. In the following, for the calculation of the brightness, we consider that the measured K_α production is within the 0.1% bandwidth (BW). We suppose that the broadening of the K_α line is of similar magnitude as measured in [27] for a conventional Mo x-ray tube source (<20 eV). Figure 2 shows the evolution of the average brightness of the x-ray source working at 100 Hz as a function of the laser intensity. It increases for intensities up to 2×10^{18} W/cm^2 and then it saturates for higher laser intensities, in the range $2–6 \times 10^{18}$ W/cm^2.

To estimate the x-ray source peak brightness, one needs to measure the x-ray pulse duration. Experimentally, the duration of the x-ray pulses in such laser plasma interaction is either measured using an x-ray streak camera which is limited to a time resolution of ∼350 fs or by pump and probe experiments [4]. The latter probes the structural changes of laser-pumped crystals with K_α pulses. In this case, the measurement corresponds to a convolution operation, and it gives only an upper limit for the duration of the x-ray pulse. Due to the atomic movement of crystals, this upper limit cannot be smaller than a few 100 fs. Ultrashort laser pulse duration and a high temporal CR are in favor for generating shorter x-ray emission duration, while a target with a high atomic number and high intensity laser will induce longer x-ray duration [8]. In this Letter, the x-ray pulse duration is not characterized. However, with the assumption of an x-ray pulse duration of $\tau_X \sim 1$ ps based on the calculation

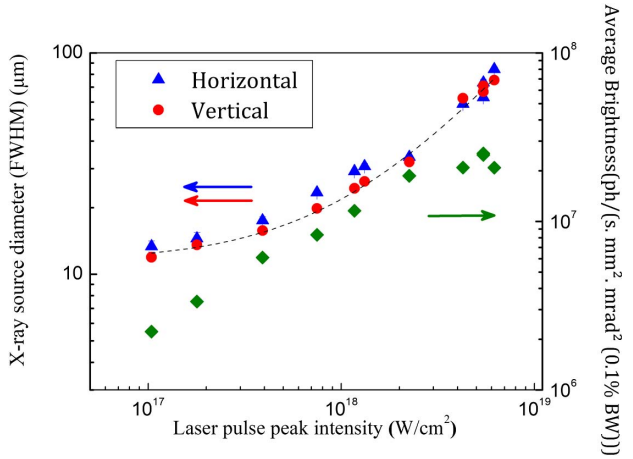


Fig. 2. Evolution of the x-ray source size (left, triangle and circle symbols for horizontal and vertical sizes, respectively) and the corresponding average brightness (right, diamond symbol) as a function of laser peak intensity. The error bars in the source size data correspond to the standard deviation of the average of the edge spread function measured for 3 different positions in the knife edge image.

[8] for bulk, a high Z element target and for 25 fs duration and a high CR 10^{10} of the laser pulse, the estimated maximum peak brightness reaches 2.5×10^{17} ph/[s·mm^2·mrad^2(0.1% BW)] at 5×10^{18} W/cm^2 laser intensity. This value of peak brightness for a laser plasma hard x-ray source is close to the one of third generation synchrotron source [10^{17}–10^{21} ph/(s·mm^2·mrad^2(0.1% BW))]. In Table 1, we finally compare the performance of our source with previous works published to date for Mo K_α production generated by laser interaction with a thick target. Table 1 shows that our source reaches the highest Mo K_α photon flux measured up to now in the context of laser-driven plasma x-ray sources with 1×10^{11} ph/(sr·s).

In summary, we report the generation of a hard (17.4 keV) and micron-sized x-ray source by the interaction of an intense femtosecond and high contrast multi-terawatt laser source working at a 100 Hz repetition rate with a thick Mo target. The K_α photon flux reaches the highest value published to date of 1×10^{11} ph/(sr·s). This Letter also shows the scaling of the K_α production as a function of laser intensity I with a power law $N_{K_\alpha}\sim I^{1.4}$ with no saturation observed. As a consequence, the estimated peak brightness of our x-ray source reaches a maximum value of $\sim2.5\times10^{17}$ ph/(s·mm^2·mrad^2(0.1% BW)) at the laser intensity of 5×10^{18} W/cm^2. Additionally, we demonstrate that the generated x-ray source at 100 Hz can combine respectively a source size of 15 μm FWHM and a photon flux of 10^9 ph/(sr·s) at $I\sim4\times10^{17}$ W/cm^2, and a source size <50 μm FWHM with a photon flux up to 10^{10} ph/(sr·s) in the intensity range of 5×10^{17}–4×10^{18} W/cm^2. These versatile characteristics are of high interest for phase contrast imaging or when a high photon flux is desirable for applications such as x-ray diffraction experiments. Further studies to improve the x-ray source efficiency will be to use thin foils and microstructured targets. Ultimately, in view of running a powerful 100 Hz laser-based x-ray source largely over minutes (≫ 1000 shots), we dispose of an available strategy [14] to pre-compensate for the reduction of the wavefront quality of the 100 Hz laser system.

Table 1. Comparison of Mo K_α Production and Conversion Efficiency Induced by Laser Interaction with a Thick Solid Target[a]

Laser Facility and X-ray Source Characteristics	CUOS-Michigan [28]	LLP-Shanghai [11]	INRS-ALLS Facility [12]	LP3-ASUR Facility (Our Source)
Laser Pulse energy (mJ)	1.3	14	245	122
Intensity (W/cm^2)	2.2×10^{18}	1.2×10^{18}	1.75×10^{18}	6.2×10^{18}
Contrast Ratio	$\sim10^6$	$\sim10^6$	$\sim10^{10}$	$\sim10^{10}$
K_α photon Number (ph/(sr·shot))	1.22×10^6	4.7×10^7	2.8×10^9	1×10^9
K_α conversion efficiency (Laser energy to K_α) in 2π sr	1.6×10^{-5}	5.7×10^{-5}	2×10^{-4}	1.3×10^{-4}
Repetition rate (kHz)	0.4	1	0.01	0.1
K_α photon number (ph/(sr·s))	4.9×10^8	4.7×10^{10}	2.8×10^{10}	1×10^{11}

[a]The table presents laser parameters for each reported work: energy, intensity, temporal CR, and repetition rate.

Funding. European Union's Horizon 2020 Research and Innovation Program (654148); LASERLAB-EUROPE; Ministry of Research and High Education; Region Provence-Alpes-Côte d'Azur; Department of Bouches-du-Rhône, City of Marseille, CNRS; Aix-Marseille University.

REFERENCES

1. R. Toth, J. C. Kieffer, S. Fourmaux, T. Ozaki, and A. Krol, Rev. Sci. Instrum. **76**, 083701 (2005).
2. T. Elsaesser and M. Woerner, J. Chem. Phys. **140**, 020901 (2014).
3. F. Dorchies, M. Harmand, D. Descamps, C. Fourment, S. Hulin, S. Petit, O. Peyrusse, and J. J. Santos, Appl. Phys. Lett. **93**, 121113 (2008).
4. A. Rousse, C. Rischel, S. Fourmaux, I. Uschmann, S. Sebban, G. Grillon, P. Balcou, E. Förster, J. P. Geindre, P. Audebert, J. C. Gauthier, and D. Hulin, Nature **410**, 65 (2001).
5. S. Fourmaux, S. Corde, K. Ta Phuoc, P. Lassonde, G. Lebrun, S. Payeur, F. Martin, S. Sebban, V. Malka, A. Rousse, and J. C. Kieffer, Opt. Lett. **36**, 2426 (2011).
6. K. Ta Phuoc, S. Corde, C. Thaury, V. Malka, A. Tafzi, J.-P. Goddet, R. C. Shah, S. Sebban, and A. Rousse, Nat. Photonics **6**, 308 (2012).
7. Y. Azamoum, V. Tcheremiskine, R. Clady, A. Ferré, L. Charmasson, O. Utéza, and M. Sentis, Sci. Rep. **8**, 4119 (2018).
8. C. Reich, "Optimization of femtosecond laser plasma kalpha sources," Ph.D. dissertation (Friedrich-Schiller-Universität Jena, 2003).
9. J. T. Bushberg, J. A. Seibert, E. M. Leidholdt, Jr., and J. M. Boone, *The Essential Physics of Medical Imaging* (Lippincott Williams & Wilkins, a Wolters Kluwer business, 2012).
10. M. Holtz, C. Hauf, J. Weisshaupt, A.-A. H. Salvador, M. Woerner, and T. Elsaesser, Struct. Dyn. **4**, 054304 (2017).
11. M. Li, K. Huang, L. Chen, W. Yan, M. Tao, J. Zhao, Y. Ma, Y. Li, and J. Zhang, Radiat. Phys. Chem. **137**, 78 (2017).
12. S. Fourmaux and J. C. Kieffer, Appl. Phys. B **122**, 162 (2016).
13. J. Wenz, S. Schleede, K. Khrennikov, M. Bech, P. Thibault, M. Heigoldt, F. Pfeiffer, and S. Karsch, Nat. Commun. **6**, 7568 (2015).
14. R. Clady, Y. Azamoum, L. Charmasson, A. Ferré, O. Utéza, and M. Sentis, Appl. Phys. B **124**, 89 (2018).
15. A. Baguckis, A. Plukis, J. Reklaitis, V. Remeikis, L. Giniūnas, and M. Vengris, Appl. Phys. B **123**, 290 (2017).
16. V. Arora, P. A. Naik, J. A. Chakera, S. Bagchi, M. Tayyab, and P. D. Gupta, AIP Adv. **4**, 047106 (2014).
17. D. Salzmann, Phys. Rev. E **65**, 056409 (2002).
18. M. Green and V. E. Cosslett, J. Phys. D **1**, 425 (1968).
19. F. Brunel, Phys. Rev. Lett. **59**, 52 (1987).
20. S. Wilks, W. Kruer, M. Tabak, and A. Langdon, Phys. Rev. Lett. **69**, 1383 (1992).
21. P. Gibbon and A. R. Bell, Phys. Rev. Lett. **68**, 1535 (1992).
22. P. Gibbon, Phys. Rev. Lett. **73**, 664 (1994).
23. Ph. Alaterre, C. Popovics, J.-P. Geindre, and J.-C. Gauthier, Opt. Commun. **49**, 140 (1984).
24. D. C. Eder, G. Pretzler, E. Fill, K. Eidmann, and A. Saemann, Appl. Phys. B **70**, 211 (2000).
25. R. B. Stephens, R. A. Snavely, Y. Aglitskiy, F. Amiranoff, C. Andersen, D. Batani, S. D. Baton, T. Cowan, R. R. Freeman, T. Hall, S. P. Hatchett, J. M. Hill, M. H. Key, J. A. King, J. A. Koch, M. Koenig, A. J. MacKinnon, K. L. Lancaster, E. Martinolli, P. Norreys, E. Perelli-Cippo, M. Rabec Le Gloahec, C. Rousseaux, J. J. Santos, and F. Scianitti, Phys. Rev. E **69**, 066414 (2004).
26. J. M. Wallace, Phys. Rev. Lett. **55**, 707 (1985).
27. J. S. Thomsen, J. Phys. B **16**, 1171 (1983).
28. B. Hou, J. Nees, A. Mordovanakis, M. Wilcox, G. Mourou, L. M. Chen, J. C. Kieffer, C. C. Chamberlain, and A. Krol, Appl. Phys. B **83**, 81 (2006).

129.104.29.1 {ts '2018-07-18 10:30:06'}